Pure Appl. Opt. **7** (1998) 393–407. Printed in the UK PII: S0963-9659(98)88692-3

Spontaneous emission and nonlinear effects in photonic bandgap materials

Ishella S Fogel, Jon M Bendickson, Michael D Tocci, Mark J Bloemer, Michael Scalora, Charles M Bowden and Jonathan P Dowling

Weapons Sciences Directorate, AMSAM-RD-WS-ST, Missile Research, Development, and Engineering Center, US Army Aviation and Missile Command, Redstone Arsenal, AL 35898-5248, USA

Received 23 October 1997

Abstract. We summarize and review our theoretical and experimental work on spontaneous emission and nonlinear effects in one-dimensional, photonic bandgap (PBG) structures. We present a new result: a method for calculating the normal-mode solutions—and hence the spontaneous emission of embedded emitters—in an arbitrary, linear, lossless, one-dimensional, PBG structure.

1. Introduction

We present results of theoretical and experimental investigations into spontaneous emission alteration and nonlinear optical effects in periodic thin-film multilayer devices—one-dimensional photonic bandgap (PBG) materials [1]. We begin with a brief section on one-dimensional photonic bandgaps and photonic band edges [1, 2]. We then introduce the concept of nonlinear optical effects in PBG structures by modelling the operation of an all-optical χ_3 PBG switch [3]. Next, we model theoretically a χ_3 thin-film device that exhibits passive anisotropic optical transmission—the optical analogue of the electronic diode [4, 5]. Next, we show, theoretically and experimentally, the enhancement of the spontaneous emission power spectrum of an emitter that is localized within a PBG structure for frequencies near the photonic band edge. This enhancement is obtained without the use of a typical microcavity [6–9]. Two slightly different AlAs–AlGaAs–GaAs, semiconductor, one-dimensional, PBG structure, light-emitting diodes (LEDs) were designed and fabricated. The emission spectra of these structures were measured and compared with that of a reference GaAs LED. We use a novel matrix-transfer method for modelling the emission rate from within the structures. Finally, we discuss some new exact analytical results for the mode density, normal-mode fields and spontaneous emission in one-dimensional PBG structures.

2. Photonic bandgaps

In the one-dimensional case, a PBG structure may be something as well known as the distributed Bragg reflector (DBR). A simple DBR consists of multiple layers of alternating

0963-9659/98/020393+15$19.50

high- and low-index materials arranged periodically. The thickness of each layer is chosen so as to satisfy the Bragg quarter-wave condition, that is

$$d = \frac{\lambda_0}{4n} \tag{1}$$

where λ_0 is the reference wavelength of the structure, and d and n are the thickness and refractive index of a particular layer, respectively. For a typical DBR, there is a range of wavelengths (called the photonic bandgap), centred about the reference wavelength λ_0, for which the structure is almost totally reflecting (that is, no propagating photon modes are allowed through the structure). Figure 1 shows a typical transmission spectrum for a DBR. The range of wavelengths demarcating the photonic bandgap is shown in the figure. It is important to note that the width of the gap is directly dependent on $\Delta n = n_H - n_L$, the refractive index difference: all other things being equal, the gap will be wider for larger

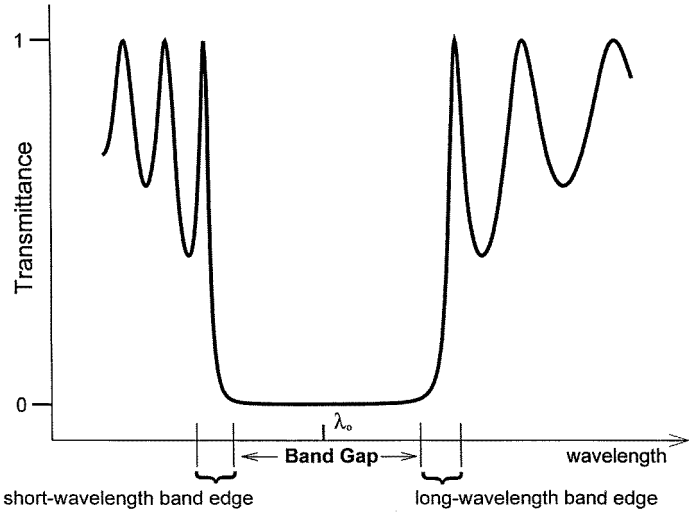

Figure 1. Typical transmission spectra $T(\lambda)$ of a one-dimensional PBG structure. Notice the three transmission resonances on either side of the gap.

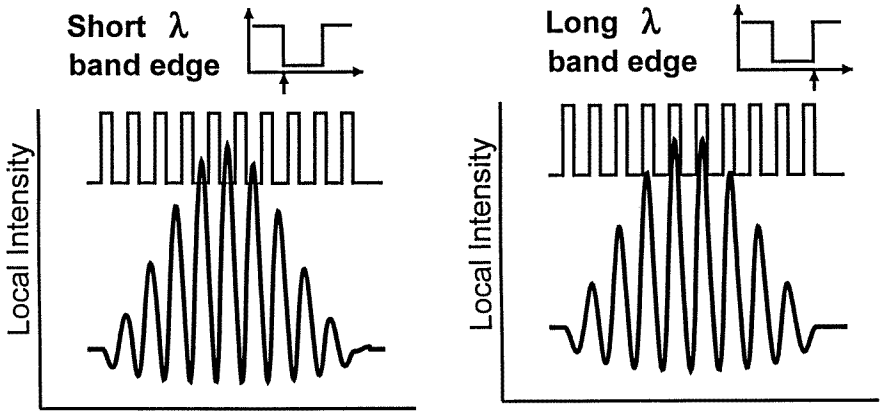

Figure 2. Local intensity at the short and long band-edge resonance wavelengths. Intensity is localized in the low- and high-index regions, respectively.

index differences [1]. (Here, n_H and n_L are the high and low refractive indices, respectively.) In this paper, we will be studying effects at wavelengths near the transmission resonances at the edges of the photonic bandgap (figure 1), as discussed in detail in [1].

Two features of optics at the photonic band edges makes these frequency regimes particularly interesting. First, is the rapid transition from poor transmission to very good transmission (that is, the steep slope of the transmission curve at the band edges), and second, is the fact that the electric fields are almost totally localized in either the high- or low-index layers. Figure 2 shows the local optical field intensity inside a typical DBR for incident plane waves—for two different cases—and illustrates this second effect.

3. Optical switch

To demonstrate the principle of operation of a PBG optical switch [3], we now consider a DBR with high-index layers which exhibit a χ_3 nonlinear optical response given by

$$n_H = n_0 + n_2 I \tag{2}$$

where n_0 is the linear refractive index, I is local intensity and n_2 is the positive nonlinear refractive index. Now consider a low-intensity *probe* beam, tuned to a wavelength corresponding to the long-wavelength band edge (see figure 3). Also consider a high-intensity *pump* beam, which is slightly detuned from the probe beam, which can be turned on or off. When the pump beam is off, the probe beam encounters a band-edge transmission resonance (full curve in figure 3), and is therefore transmitted. When the pump beam is turned on, the high-intensity pump light will be localized in the high-index layers, the refractive indices of which increase with high intensity, and so the gap widens (see the broken curve in figure 3). Now the probe beam encounters a highly reflecting structure, and so is not transmitted. Thus the probe beam may be controlled (effectively turned on or off after the PBG structure) by turning the pump beam on or off [3].

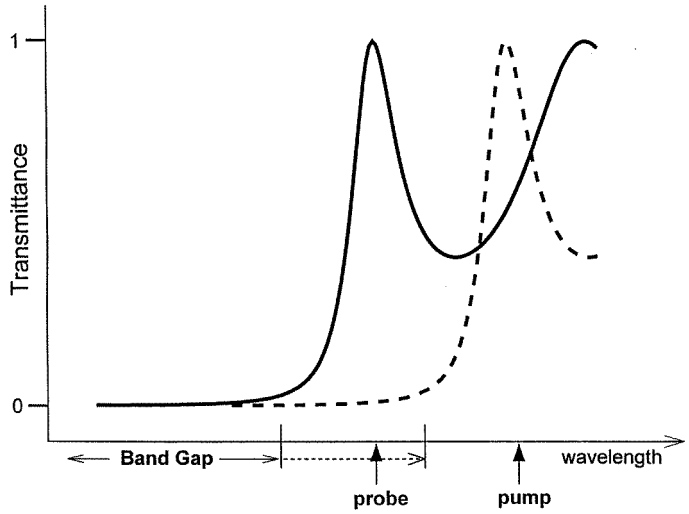

Figure 3. An optical switch: the bandgap widens as the intensity of the incident pump radiation increases.

4. Optical diode

The method of operation of the optical diode is similar to that of the switch described previously [4]. We begin again with a χ_3 nonlinear DBR. This time, however, the index of each period after the first is increased by a small amount over the previous period. The result is a ramped-index DBR, as shown in figure 4. Because the indices in the first few periods on the left-hand side are lower than those in the first few periods on the right-hand side, the left-hand side of the structure can be said to have a *local photonic band edge* that is at a shorter wavelength than the right-hand side of the structure. In other words, for some specific wavelength of incident light, the portion of the ramped DBR on the right-hand side of the figure is highly reflecting, while the portion on the left-hand side is highly transmitting. Thus, light incident from the left may indeed penetrate further into the structure before being

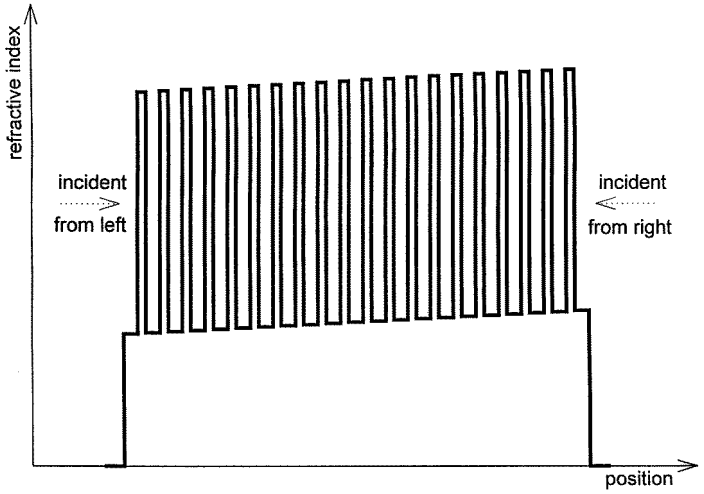

Figure 4. An optical diode configuration: the linear index ramp is accompanied by a χ_3 nonlinearity.

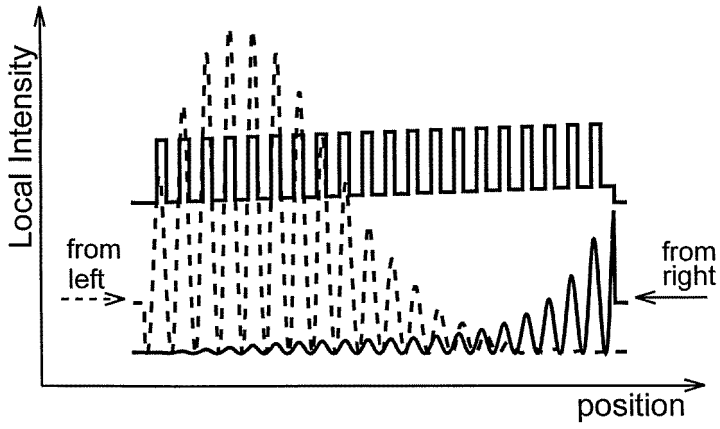

Figure 5. The local intensity in the linear diode is dependent on the direction of incidence—the key to its operation.

reflected than would light incident from the right, as can be seen in figure 5, produced by a nonlinear matrix transfer code [5]. Figure 5 shows the localized intensity inside a *linear* ramped index structure. Note that for light incident from the left, the intensity is localized in the high-index layers and that there is strong optical-field enhancement in the first several periods. For light incident from the right, not only is the field enhancement comparatively weak, but the field is localized in *between* the high and low layers, as expected for a good DBR reflector. Thus, by introducing an optical nonlinearity into the high-index layers (one with a negative n_2), we may now allow the light incident from the left to dynamically shrink the width of the bandgap (by lowering the index of the high-index layers) as it propagates, while nearly preventing light incident from the right from doing so. Thus, high-intensity light, of a specific wavelength, incident from the left would be more apt to be transmitted through the structure than the same type of light incident from the right.

Some of the present authors predicted that this type of diode action is, in fact, generally possible for the special case of incident pulses [4]. Figure 6 shows the main result from this study; a significant fraction of a right-moving pulse is transmitted, while nearly all of a left-moving pulse is reflected.

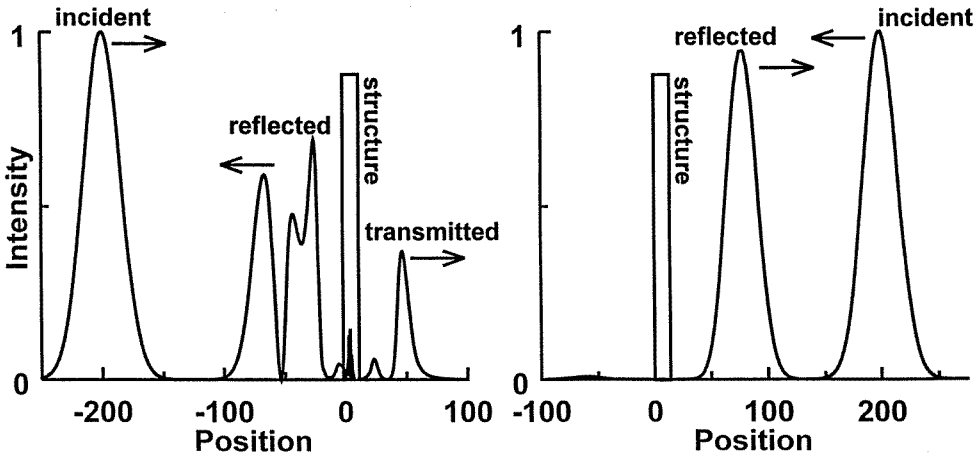

Figure 6. Diode operation for pulses: much of the high-intensity pulse incident from the left is transmitted, while that from the right is reflected.

In a later publication, our group then used actual material parameters and a specially modified matrix transfer method to model plane waves incident onto a physically realizable χ_3 nonlinear optical diode structure [5]. This study used parameters for a polydiacetylene (9-BCMU) and rutile (TiO_2) and incident intensity values that were of the order of 10 MW cm^{-2}. While we confirmed the results of the previous studies, our investigation also showed that a ramp in the index profile was not necessary. In part, we found that ramping the index was analogous to increasing the *optical thickness* of the layers across the structure, which could simply be accomplished by increasing the *thickness* of each layer across the structure, rather than increasing the index. This innovation loosened the stringent fabrication requirements demanded by the optical diode. In this study, it was the low-index layers that exhibited the nonlinearity, and so it was the short-wavelength band edge that was the region of interest. In figure 7, the full curve in the figure is the transmission spectrum of the structure, for low light intensities (linear case), in the spectral region of the short-wavelength band edge. The short-broken curve is the transmittance spectrum for

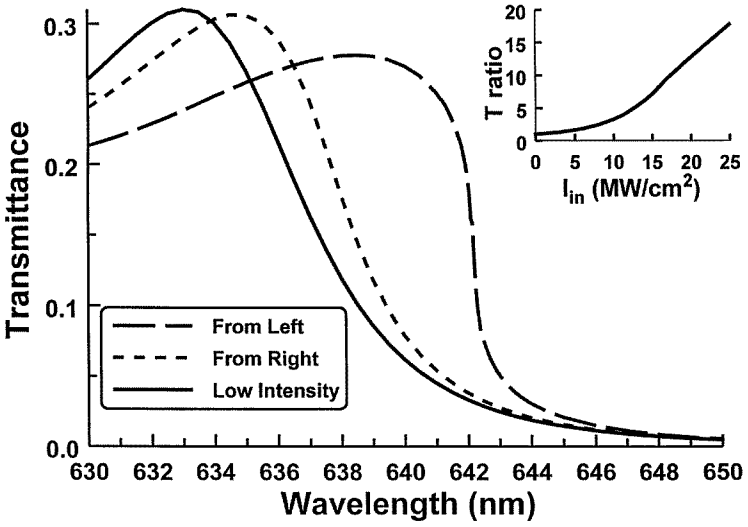

Figure 7. The steady-state nonlinear matrix-transfer calculation at 13 MW cm^{-2} indicates anisotropic transmittance $T(\omega)$ for right- and left-incident radiation. The low-intensity (full) curve is the same for both directions.

light incident from the right at 13 MW cm^{-2} and the long-broken curve is the transmittance spectrum for light incident from the left at the same intensity. An important implication of this figure is that for a wavelength of about 641 nm (and an input intensity of 13 MW cm^{-2}), light incident from the left will experience approximately 25% transmittance through the structure, while light incident from the right will experience only 5% transmittance. Thus we realize five times as much transmitted light through the structure for light incident from the left as for light incident from the right. As the inset of figure 7 shows, the ratio of left to right transmittance through the structure increases with increasing intensity. Another interesting note is that for intensities greater than around 15 MW cm^{-2}, the device exhibits optical bistability for light incident from the left *only*.

In recent work we found that a ramp in the optical thickness of the layers across the structures was not necessary to realize optical diode behaviour. We found that practically *any* directional asymmetry in the design of the structure led to an asymmetry in the left- to right-incident field profiles. By testing many different structures, we found that the deposition of a single thin film with carefully chosen index and thickness, on top of a symmetric structure could lead to wildly different left- and right-incident field profiles. For example, a single layer of rutile ($n = 2.7$), with an optical thickness of 0.15 of a wavelength, on one side of an otherwise symmetric AlAs–GaAs DBR led to nearly six times as much localized intensity in the high-index layers for light incident from one direction than for light incident from the opposite direction. Difficulties in growing many layers of rutile and polydiacetylene have hindered the experimental demonstration of this effect. We are seeking materials with as good nonlinear refractive index and absorption, but better fabrication properties.

5. Spontaneous emission

In a paper by two of the authors (JPD and CMB), the prediction was made that the spontaneous emission spectrum of a radiating dipole embedded inside a PBG structure

would be altered so as to be enhanced (compared to its free-space radiation power) at frequencies near the photonic band-edge resonance [1, 6, 7]. A numerical analysis by our group confirmed this theoretical finding, and set the stage for our most recent experimental work [9]. Another result from [6] is a semiclassical derivation of the following expression for the emission power spectrum for the embedded point dipole emitting at a frequency ω and located at a position x:

$$P(\omega, x) = C\rho(\omega)|a(\omega, x)|^2 \tag{3}$$

where $\rho(\omega)$ is the density of the photon modes, $a(\omega, x)$ is the value of the electric-field normal modes at the position of the dipole, which both depend on the frequency ω, and C is a constant that is possibly ω dependent and that depends on, among other things, the material parameters of the emitting dipole (there have been other, quantum electrodynamical derivations of this expression [8]). To eliminate the constant C from our calculations, we used a parameter that we call the emission enhancement, I_{enh}, which is simply the ratio of the emitted power spectrum of a PBG test sample to that of a reference sample:

$$I_{\text{enh}} = \frac{P(\omega)^{\text{PBG}}}{P(\omega)^{\text{ref}}}. \tag{4}$$

Thus, by measuring the power spectra of a one-dimensional PBG test sample and that of a similar reference sample, an *experimental* value for the emission enhancement could be obtained. Meanwhile, by calculating the density of modes and the normal-mode field for both the test sample and the reference sample, a *calculated* value for the emission enhancement could be obtained. In this way a good comparison may be made between the theory and the results from the experiment. A brief explanation of both the experimental and modelling procedures is given here, but a more complete description may be found in [9].

Both the normal-mode field $a(\omega, x)$ and the density of modes $\rho(\omega)$ were found using a standard matrix transfer method for calculating the electric field inside stratified media [1, 10]. By dividing the intensity of the electric field by the total energy under the curve, the electric field mode was normalized:

$$|a(\omega, x)|^2 = \frac{|E(\omega, x)|^2}{\int_0^D n^2(x)|E(\omega, x)|^2 \,\mathrm{d}x} \tag{5}$$

where x is the direction perpendicular to the interfaces, and 0 and D are the initial and final x coordinates of the structure, respectively, and $n(x) \in \{n_{\text{H}}, n_{\text{L}}\}$ is the spatially varying refractive index. Furthermore, the value of the normal-mode-field-squared was averaged over the region of the emitted layer:

$$\left\langle |a(\omega)|^2 \right\rangle = \frac{\int_a^b |a(\omega, x)|^2 \,\mathrm{d}x}{(b-a)} \tag{6}$$

where a and b are the initial and final x coordinates of the emitting layer, respectively. Now, assuming light incident onto the structure from the left, the transmission coefficient of the structure is simply the ratio of the right-travelling electric field just to the right of the structure (E_{out}) to the right-travelling electric field just to the left of the structure (E_{in}). This number is, in general, complex, and so it may be written equally well in either polar or Argand notation:

$$t(\omega) = \frac{E_{\text{out}}}{E_{\text{in}}} = \sqrt{T}\,\mathrm{e}^{\mathrm{i}\phi} = u(\omega) + \mathrm{i}v(\omega) \tag{7}$$

where $t(\omega)$ is the transmission coefficient as a function of frequency, $\sqrt{T}$ and ϕ are the amplitude and phase of t, respectively, and u and v are the real and imaginary parts of t, respectively, where we define $T \equiv |t|^2$. The phase of the transmission coefficient may be thought of as the phase accumulated by a plane wave as it traverses the structure. If the structure's total thickness is D, then an effective wavenumber k_{eff} may be introduced such that the phase thickness of the structure is equal to the product of the effective wavenumber and the structure's thickness:

$$\phi = k_{\text{eff}} D. \tag{8}$$

Rewriting this in terms of the real and imaginary parts of t yields

$$\tan[k_{\text{eff}} D] = \frac{v}{u} \tag{9}$$

which may then be written as a dispersion relation as follows:

$$k_{\text{eff}}(\omega) = \frac{1}{D} \tan^{-1}\left[\frac{v(\omega)}{u(\omega)}\right]. \tag{10}$$

Now, the one-dimensional density of modes is simply the magnitude of the derivative of the wavenumber with respect to frequency,

$$\rho(\omega) = \left|\frac{\mathrm{d}k}{\mathrm{d}\omega}\right| = \frac{1}{D}\left|\frac{u'v - v'u}{u^2 + v^2}\right| \tag{11}$$

where the primes denote derivatives with respect to frequency.

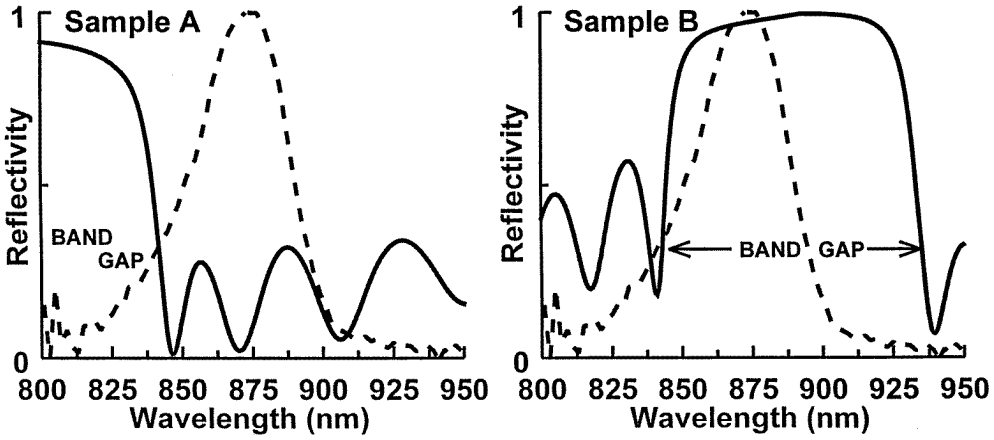

Figure 8. Design strategies for samples A and B in our experiment. Full curves are the calculated reflectivity of samples with respect to the GaAs LED emission spectrum (broken curve).

For the experiment, we designed two different PBG test samples and used one reference sample. All of the samples were designed as p–i–n doped AlAs–AlGaAs–GaAs surface-emitting LEDs, with GaAs as the emitter. For an emitter embedded in a high-index layer (as we have in this case), the theory predicts that the emission will be enhanced at the long-wavelength band edge more than at the short-wavelength band edge, since here the electric-field intensity at the location of the dipole is largest. Also, the emission should be suppressed at frequency ω inside the photonic bandgap. With these ideas in mind, we designed the first PBG test sample (called sample A) to have its long-wavelength band edge overlapping with the reference GaAs emission spectrum, with more of the reference

spectrum lying outside the bandgap than inside it (figure 8, left). We designed the second PBG test sample (called sample B) to have its short-wavelength band edge overlapping with the reference spectrum, with more of the reference spectrum lying inside the bandgap than outside it (figure 8, right). According to the theory, sample A should emit far more radiation than sample B. Figure 9 is a schematic diagram of the structure of samples A and B. Both test samples consisted of 20.5 periods of $Al_{x=0.2}GaAs$ and AlAs, with the central AlGaAs layer replaced by an emitting GaAs layer. With the exception of the p-cap, the optical thickness of each layer is exactly one quarter of a wavelength (for some reference wavelength). The two test samples were identical in form; only the actual thicknesses of the layers were different (corresponding to different reference wavelengths for the two samples). A three-layer $Al_{0.4}Ga_{0.6}As$–GaAs–$Al_{0.4}Ga_{0.6}As$ p–i–n light-emitting diode was used as a reference sample—corresponding to a control bulk emitter. Each layer in the reference sample had a thickness much greater than a vacuum wavelength (~ 875 nm) corresponding to the peak of the GaAs emission, and so quantum-confinement effects are negligible.

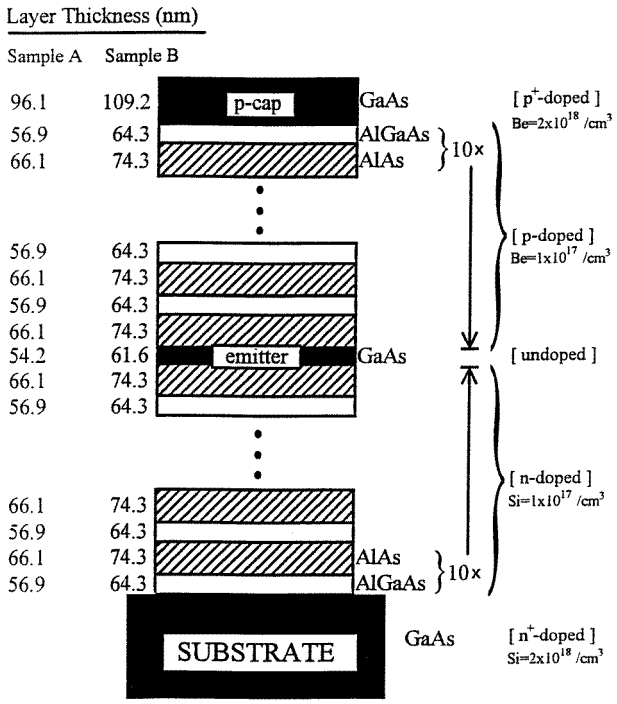

Figure 9. Schematic diagram of samples A and B. The emitter layer is also a quarter-wave layer, i.e. there is no $\lambda/2$ or λ cavity.

Figure 10 shows a comparison between the measured and calculated emission enhancements. The close agreement between the shapes of the spectral enhancements of the matrix-transfer calculation and measurement is easily seen. Because of the very different characteristics of the test samples and those of the reference sample, both of the measured emission enhancements were divided by the same constant number. The relative heights and shapes of the two curves were not changed.

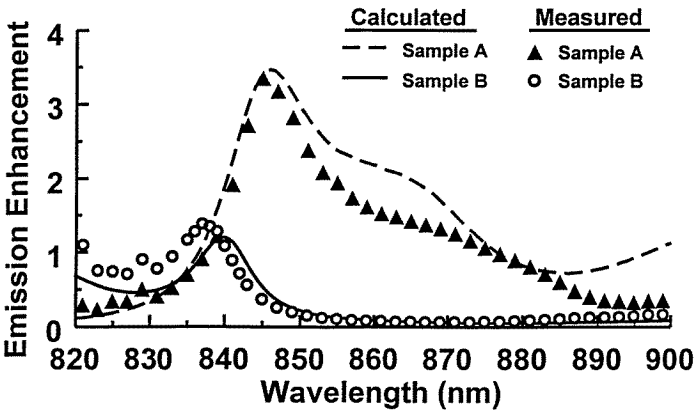

Figure 10. Measured and calculated emission enhancements. An enhancement of 1 corresponds to no enhancement—the emissivity of the bulk material.

The *measured* emission enhancement of each PBG sample was found by dividing the emission spectrum of each PBG sample by that of the reference sample (see equation (4)). Since the reference sample had an intrinsic layer thickness and current–voltage characteristic different from the two PBG samples, we could not directly compare the absolute emission power of the reference sample with those of the PBG samples. It was necessary to scale the measured PBG sample emission spectra by some constant number (the same scaling number was used for samples A and B). We chose an injection current through the reference sample of 63 mA, but we found that varying the current (from 18–78 mA) did not alter the shape of the measured surface-emission enhancement. This insensitivity to the injection current is due to the broad emission spectrum of the reference sample.

6. Analytical results

In the previous section, we saw that a numerical matrix transfer code could be used to calculate the spontaneous emission power $P(\omega, x)$ (equation (3)), in a one-dimensional quasi-PBG structure, giving excellent agreement with experiment. In actual devices, we rarely have an exactly periodic structure, due to the DBR substrate, the active quarter-wave region, etc. However, much can be learned and analytical results can be obtained assuming a lossless, exactly periodic one-dimensional PBG structure. For example, an exact expression for the density of modes, $\rho(\omega)$, equation (11), can be obtained [1].

Consider figure 11(a), where we show the transmission of light through a linear, lossless, refractive index profile $n(x)$ on the compact domain (a, b), of length $d = b-a$. The complex transmittance $t(\omega) = u(\omega) + \mathrm{i}v(\omega)$ is given by equation (7), and the mode density $\rho(\omega)$, by equation (11). Let us assume that $t(\omega)$ can be calculated for this index profile $n(x)$, either analytically or numerically. Let us now assume that this potential $n(x)$ is repeated N times to form an exactly periodic index profile, as shown in figure 11(b). The finite periodic structure has N periods and length $D = Nd = N(b - a)$. We now wish to compute the complex transmittance, $t_N = u_N + \mathrm{i}v_N$, of the stack in terms of that of the single period. Let us suppose that the transfer matrix for the single period in figure 11(a) is given by $\hat{\mathbf{M}}$,

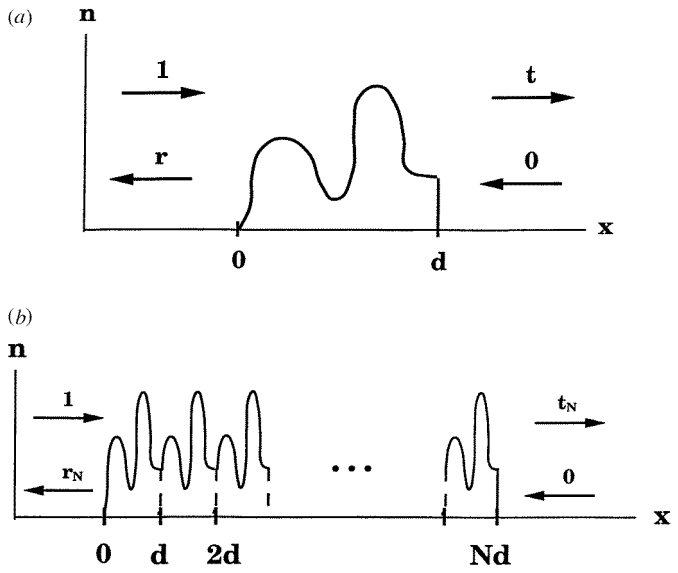

Figure 11. In (*a*) we show the transmittance t and reflectance r of a one-dimensional unit cell with index variation $n(x)$. In (*b*) we repeat the unit cell N times to make a finite one-dimensional PBG.

implicitly defined by

$$\begin{bmatrix} 1 \\ r \end{bmatrix} = \hat{\mathbf{M}} \begin{bmatrix} t \\ 0 \end{bmatrix} \tag{12}$$

where r is the complex reflectance. We are assuming that an optical field of electric field amplitude 1 is incident from the left, and no field from the right, as in figure 11(*a*). From energy conservation and time-reversal symmetry, it can be shown that $\hat{\mathbf{M}}$ has the very general form [1]

$$\hat{\mathbf{M}} = \begin{pmatrix} 1/t & r^*/t^* \\ r/t & 1/t^* \end{pmatrix} \tag{13}$$

where the asterisk denotes complex conjugation. The eigenvalue equation for $\hat{\mathbf{M}}$ is easily seen from equation (13) to be $\mu^2 - 2\mu\,\mathrm{Re}\{1/t\} + 1 = 0$, where the two eigenvalues $\mu^{\pm}$ are related by $\mu^+\mu^- = \det|\hat{\mathbf{M}}| = 1$ by unimodularity.

We would now like to make a very important point. Suppose, for the sake of discussion, we were to impose the periodic boundary condition, $n(x) = n(x + d)$, for $x \in (-\infty, \infty)$, and then seek the corresponding Bloch eigenfunctions $\boldsymbol{u}_{\mathrm{B}}$, appropriate for an *infinite*-period potential with unit cell $n(x)$, $x \in (0, d]$. We know that the Bloch functions change only in phase, and not in amplitude, from cell to cell in the infinite periodic potential. This phase-per-unit-cell is called the *Bloch phase* β, associated with the infinite periodic structure. For these Bloch eigenfunctions, $\boldsymbol{u}_{\mathrm{B}}$, we have then, from the definition of an *eigenvector*, the *eigenvector equation* $\hat{\mathbf{M}}\boldsymbol{u}_{\mathrm{B}} = \mu_{\mathrm{B}}^{\pm}\boldsymbol{u}_{\mathrm{B}} = \mathrm{e}^{\pm \mathrm{i}\beta}\boldsymbol{u}_{\mathrm{B}}$, where the last term comes from the definition of the Bloch phase β. Hence, the eigenvalues for the Bloch functions are of the form $\mu_{\mathrm{B}}^{\pm} = \mathrm{e}^{\pm \mathrm{i}\beta}$, since $\mu_{\mathrm{B}}^{+}\beta_{\mathrm{B}}^{-} = 1$. Now, since the eigenvalue equation holds for all eigenvalues μ of $\hat{\mathbf{M}}$, in particular, it holds for the Bloch eigenvalues $\mu_{\mathrm{B}}^{\pm}$. Inserting

$\mu_{\mathrm{B}}^{\pm} = \mathrm{e}^{\pm \mathrm{i}\beta}$ into the eigenvalue equation, and equating real and imaginary terms, yields the very important relation that

$$\mathrm{Re}\,\{1/t\} = \cos\beta \tag{14}$$

where β is again the Bloch phase for the hypothetical infinite periodic structure.

From the Cayley–Hamilton theorem, one can show that the unit cell transfer matrix $\hat{\mathbf{M}}$, equation (13), obeys its own eigenvalue equation, namely

$$\hat{\mathbf{M}}^2 - 2\hat{\mathbf{M}}\cos\beta + \hat{\mathbf{I}} = 0 \tag{15}$$

where $\hat{\mathbf{I}}$ is the 2×2 identity matrix, and $\beta = \beta(\omega)$ is the Bloch phase. Now the transfer matrix for the entire N-period stack, figure 11(b), is simply the product of the matrices of the unit cells, i.e. $\hat{\mathbf{M}}_N = \hat{\mathbf{M}}^N$. Using the matrix-valued eigenvalue equation (15), we can prove by induction that [1]

$$\hat{\mathbf{M}}^N = \hat{\mathbf{M}}\frac{\sin N\beta}{\sin\beta} - \hat{\mathbf{I}}\frac{\sin(N-1)\beta}{\sin\beta}. \tag{16}$$

This is an extremely important result, in that it expresses the transfer matrix of the stack, $\hat{\mathbf{M}}^N$, in terms of $\hat{\mathbf{M}}$, β and N. Since $\hat{\mathbf{M}}$ is assumed to be known for the unit cell, hence β is also known, and we have an expression for the N-period stack in terms of N and the properties of the unit cell. The stack matrix $\hat{\mathbf{M}}_N = \hat{\mathbf{M}}^N$ also obeys the general form

$$\hat{\mathbf{M}}^N = \begin{pmatrix} 1/t_N & r_N^*/t_N^* \\ r_N/t_N & 1/t_N^* \end{pmatrix} \tag{17}$$

where t_N and r_N are the complex transmittance and reflectance of the entire stack (see figure 11(b)). Combining equations (16) and (17), we get

$$\frac{1}{t_N} = \frac{1}{t}\frac{\sin N\beta}{\sin\beta} - \frac{\sin(N-1)\beta}{\sin\beta} \tag{18a}$$

$$\frac{r_N}{t_N} = \frac{r}{t}\frac{\sin N\beta}{\sin\beta} \tag{18b}$$

which now gives us the complex transmittance and reflectance of the periodic stack, t_N and r_N, respectively, in terms of N and known properties t, r and β of the single unit cell. If we define the transmission functions for the unit cell and the stack by $T \equiv |t|^2$ and $T_N \equiv |t_N|^2$, we may use equations (18) to obtain

$$\frac{1}{T_N} = 1 + \frac{\sin^2 N\beta}{\sin^2\beta}\left[\frac{1}{T} - 1\right] \tag{19}$$

from which we see that the stack is transparent, $T_N = 1$, whenever either $T = 1$ or whenever $N\beta$ is an integer multiple of π. The latter case corresponds to the transmission resonances of the stack as depicted in figure 1.

Using equations (18), combined with equation (11) for the density of modes ρ, we may derive an exact analytical expression for the density of modes for the stack,

$$\rho_N(\omega) = \frac{1}{D}\frac{\left[\sin^2 N\beta/(2\sin\beta)\right]\left[\eta' + \eta\xi\xi'/\left(1-\xi^2\right)\right] - N\left(\eta\xi'/\left(1-\xi^2\right)\right)}{\cos^2 N\beta + \eta^2\left[\sin^2 N\beta/\left(\sin^2\beta\right)\right]} \tag{20}$$

where we have defined $\xi \equiv u/T$ and $\eta = v/T$, and where $t = u + \mathrm{i}v$ is the unit cell transmittance and $T \equiv |t|^2$. Here the prime denotes differentiation with respect to ω. Once again, the expression ρ_N for the N-period stack is given entirely in terms of properties of the unit cell.

Now we have almost enough information for an exact analytical expression for the spontaneous emission power $P_n(\omega, x)$, equation (3), of a dipole in the nth unit cell at position x and frequency ω. Such an expression corresponds to a new result. We have $\rho_N(\omega)$, and now we need the normal-mode function $a_n(\omega, x)$ as a function of the position x in the nth cell. We describe here, for the first time, how to compute this. Consider figure 11(*b*), where the boundary conditions are 1 and r_N on the left of the stack and t_N and 0 on the right. All these quantities are known, equation (18), and hence, in principle, determine the field anywhere inside the stack uniquely. Let us consider a generic arbitrary unit cell in the N-period stack, call it the nth cell with $n = 1, 2, 3, \ldots, N$. The form of the right- and left-propagating electric fields, $E^{\pm}(x)$, in a given unit cell is assumed to be known from the solutions of Maxwell's equations for the unit cell. (For example, if the unit cell has a linear index ramp $n(x) = a + bx$, then $E^{\pm}(x)$ are expressible in terms of the two independent Airy functions $\mathrm{Ai}(x)$ and $\mathrm{Bi}(x)$.) Hence, the general form of the electric field in the nth cell, $E_n(\omega, x)$, has the form

$$E_n(\omega, x) = A_n(\omega)\, E^+(x) + B_n(\omega)\, E^-(x) \tag{21}$$

where $A_n(\omega)$ and $B_n(\omega)$ depend on ω but are independent of x and are uniquely determined by the boundary conditions r_N and t_N on the edges of the stack, as well as the number n. The *inverse* of the partial-stack transfer matrix $\hat{\mathbf{M}}^{n-1}$ propagates the left-stack boundary condition $\left[\begin{smallmatrix}1\\ r_N\end{smallmatrix}\right]$ to the right-hand side of the nth unit cell, and the matrix $\hat{\mathbf{M}}^{N-n}$ propagates the right-stack condition $\left[\begin{smallmatrix}t_N\\ 0\end{smallmatrix}\right]$ to the right-hand side of the same nth unit cell. (A matrix $\hat{\mathbf{M}}^m$ propagates right-to-left and its *inverse* propagates left-to-right.) Equation (16) can be used to reduce $\hat{\mathbf{M}}^{n-1}$ and $\hat{\mathbf{M}}^{N-n}$ to a function of only N and the unit cell quantities $\hat{\mathbf{M}}$ and β. When we are done, we have an expression for $A_n(\omega)$ and $B_n(\omega)$, and hence $E_n(\omega, x)$, in terms of n, N and properties of the elementary unit cell. The expression is too lengthy to give in full here, and will be presented in a future work [11]. This is the first analytic expression for the electric normal modes in a finite one-dimensional PBG, and as a consequence of equation (20) for the density of modes, and equation (3), an exact analytic expression for the spontaneous emission of an emitter embedded in a finite, one-dimensional periodic structure.

The only remaining point to connect the electric field modes $E_n(\omega, x)$, equation (21), to the modes $a_n(\omega, x)$ used in the spontaneous emission calculation, is to normalize the modes $E_n(\omega, x)$ to the total energy in the field. The general form of this normalization is given by equation (5), where the denominator represents the Maxwell electric-field energy density U_N in the structure [6]. For our periodic structure, this simplifies to

$$\begin{aligned} U_N(\omega) &= \int_0^{Nd} n^2(x)\, |E(\omega, x)|^2 \, \mathrm{d}x \\ &= \sum_{n=1}^{N} \int_{(n-1)d}^{nd} n^2(x)\, |E_n(\omega, x)|^2 \, \mathrm{d}x \\ &\equiv \sum_{n=1}^{N} U_n(\omega) \end{aligned} \tag{22}$$

where $E_n(\omega, x)$ is given by equation (21), and $U_n(\omega)$ is the electric-field energy density in the nth unit cell. We can now compute the correctly normalized normal modes $a_n(\omega, x)$ in the nth unit cell, namely

$$a_n(\omega, x) = \frac{E_n(\omega, x)}{\sqrt{U_N(\omega)}} \tag{23}$$

or, in other words, we are normalizing the modes to the total electric-field energy U_N inside the N-period stack. Hence we have a prescription for computing $a_n(\omega, x)$ analytically, given $E_n(\omega, x)$ in equation (21).

For a point dipole in the nth cell oscillating at frequency ω and located at a position x in the stack, with $(n-1)d < x \leqslant nd$, the spontaneous emission power emitted on axis, $P_n(\omega, x)$, is proportional to the one-dimensional spontaneous emission rate γ and is given as in equation (3) as

$$P_n(\omega, x) = C\rho_N(\omega)\,|a_n(\omega, x)|^2 \tag{24}$$

where $a_n(\omega, x)$ is given by equation (23) and $\rho_N(\omega)$ is given by equation (20). For a point dipole oscillating at frequency ω, the radiating current density $J(x, t)$ has the form

$$J = \omega p \cos(\omega t)\,\delta(x) \tag{25}$$

where p is the dipole moment [6]. For such a radiating element, we have [6]

$$C = \tfrac{1}{2}\pi^2\omega^2 p^2 \tag{26}$$

which completes the analytical analysis of this one-dimensional model.

7. Conclusion

We have shown results of several investigations into some of the interesting band-edge phenomena associated with PBG structures. We began by demonstrating the principle of operation of the nonlinear band-edge optical switch [3]. We then introduced the nonlinear thin-film optical diode and showed results from numerical investigations into the problem [4, 5]. It was shown numerically that more than five times as much transmission in one direction as in the opposite direction should be possible using realistic materials and intensities. Then, we gave results from an experimental investigation into spontaneous emission alteration at the photonic band edge. A novel numerical method for calculating such an emission alteration was also presented and we showed that it accurately predicts the experimental results. Finally, we showed how the density of modes and, for the first time, how the optical normal modes of an exactly periodic, one-dimensional, PBG structure may be obtained analytically. This result gives an exact, closed-form expression for the atomic spontaneous emission rate in such a one-dimensional structure. The ability to alter and model the spontaneous emission of active media in such a way may find important new applications in such fields as flat-screen LED displays and high-efficiency LEDs.

References

[1] Bendickson J M, Dowling J P and Scalora M 1996 Analytic expressions for the electromagnetic mode density in finite, one-dimensional, photonic band-gap structures *Phys. Rev.* E **53** 4107

[2] Yariv A and Yeh P 1984 *Optics in Crystals* (New York: Wiley–Interscience)

[3] Scalora M, Dowling J P, Bowden C M and Bloemer M J 1994 Optical limiting and switching of ultrashort pulses in nonlinear photonic band-gap materials *Phys. Rev. Lett.* **73** 1368

[4] Scalora M, Dowling J P, Bowden C M and Bloemer M J 1994 The photonic band edge optical diode *J. Appl. Phys.* **76** 2023

[5] Tocci M D, Bloemer M J, Scalora M, Dowling J P and Bowden C M 1995 A thin-film nonlinear optical diode *Appl. Phys. Lett.* **66** 2324

[6] Dowling J P and Bowden C M 1992 Atomic emission rates in inhomogeneous media with applications to photonic band structures *Phys. Rev.* A **46** 612

[7] Scalora M, Dowling J P, Tocci M D, Bloemer M J, Bowden C M and Haus J W 1995 Dipole emission rates in one-dimensional photonic band-gap materials *Appl. Opt.* B **60** S57

[8] Glauber R J and Lewenstein M 1991 Quantum optics of dielectric media *Phys. Rev.* A **43** 467
[9] Tocci M D, Scalora M, Bloemer M J, Dowling J P and Bowden C M 1996 Measurement of spontaneous emission rates near the one-dimensional photonic band edge of semiconductor heterostructures *Phys. Rev.* A **53** 2799
[10] Born M and Wolf E 1980 *Principles of Optics* (Oxford: Pergamon)
[11] Fogel I S and Dowling J P 1998 *Phys. Rev.* A to be submitted